Fabrication of eco-friendly nanocellulose-chitosan-calcium Phosphate ternary nanocomposite for wastewater remediation

Sherin Peter, Nathalie Lyczko, Sabu Thomas, Denis Leruth, Alain Germeau, Dorina Fati, Ange Nzihou

Chemosphere 363 (2024) 142779

Contents lists available at ScienceDirect

Chemosphere

journal homepage: www.elsevier.com/locate/chemosphere

Fabrication of eco-friendly nanocellulose-chitosan-calcium phosphate ternary nanocomposite for wastewater remediation

Sherin Peter [a], Nathalie Lyczko [a], Sabu Thomas [b], Denis Leruth [c], Alain Germeau [c], Dorina Fati [c], Ange Nzihou [a,*]

[a] Université de Toulouse, IMT Mines Albi, RAPSODEE CNRS UMR-5302, Campus Jarlard, Albi cedex 09, F-81013, France
[b] International and Inter-University Centre for Nanoscience and Nanotechnology, and School of Energy Studies, Mahatma Gandhi University, Kottayam, 686 560, India
[c] PRAYON S.A., Rue J. Wauters, 144, B-4480, Engis, Belgium

HIGHLIGHTS

- Cost-effective, green approach to the nanocomposite synthesis.
- Usage of biowaste derivates and inorganic materials for green development.
- Hybrid approach of combining adsorption and size exclusion with optimized formulations for outstanding performance.
- The nanocomposite achieved up to 98.7% removal of Ni ions and 100% removal of Congo red (CR) dye.
- Efficient removal of heavy metals (Cd, Ag, Al, Fe, Hg, Mo, Li, Se) and other elements (Ba, Be, P, Zn) from real-world municipal wastewater.

GRAPHICAL ABSTRACT

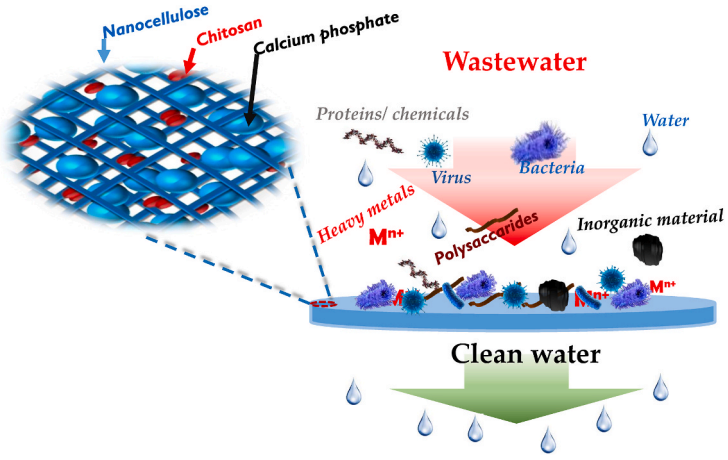

ARTICLE INFO

Handling editor: Y Yeomin Yoon

Keywords:
Wastewater treatment
Nanocomposite
Membrane filtration
Green approach
Pollutants removal

ABSTRACT

Nanocomposites have emerged as promising materials for pollutant removal due to their unique properties. However, conventional synthesis methods often involve toxic solvents or expensive materials. In this study, we present a novel ternary nanocomposite synthesized via a simple, cost-effective vacuum filtration method. The composite consists of calcium phosphate (CaP), biowaste-derived nanocellulose (diameter <50 nm) (NC), and chitosan (CH). The nanocomposite exhibited exceptional pollutant removal capabilities due to the hybrid approach of combining adsorption and size exclusion that widens and accelerates pollutant removal. When tested with synthetic wastewater containing 10 ppm of Ni ions and 10 ppm of Congo red (CR) dye, it achieved impressive removal rates of 98.7% for Ni ions and 100% for CR dye. Moreover, the nanocomposite effectively removed heavy metals such as Cd, Ag, Al, Fe, Hg, Mo, Li, and Se at 100%, and Ba, Be, P, and Zn at 80%, 92%, 87%, and 97%, respectively, from real-world municipal wastewater. Importantly, this green nanocomposite

* Corresponding author. Université de Toulouse, IMT Mines Albi, RAPSODEE CNRS UMR-5302, Campus Jarlard, F-81013, Albi cedex 09, France.
E-mail addresses: sherinpeter2804@gmail.com (S. Peter), Nathalie.lyczko@mines-albi.fr (N. Lyczko), sabuthomas@mgu.ac.in (S. Thomas), dleruth@prayon.com (D. Leruth), agermeau@prayon.com (A. Germeau), dfati@prayon.com (D. Fati), ange.nzihou@mines-albi.fr (A. Nzihou).

https://doi.org/10.1016/j.chemosphere.2024.142779
Received 27 May 2024; Received in revised form 1 July 2024; Accepted 4 July 2024
Available online 5 July 2024

membrane was synthesized without the use of harmful chemicals or complex modifications and operated at a high flux rate of 146 L/m^2.h.MPa. Its outstanding performance highlights its potential for sustainable pollutant removal applications.

1. Introduction

Increasing human activities for enhancing agricultural and industrial production and lifestyle changes have resulted in increased pollutant deposition in the water bodies (Nayak and Bhushan, 2021). These pollutants ending up in the water resources forced the authorities such as the United Nations to introduce sustainability policies that aim to ensure the availability and management of water and sanitation ("Water and wastewater treatment technologies," n. d.). Depending on the nature, type, and concentration of the pollutants in the water bodies and their degradation pathways, different pollutants exhibit different toxicity effects on the environment and living organisms (Huang et al., 2020; Kumar et al., 2020) Heavy metals like arsenic originated from industries related to glass, pigments, textiles, paper, and metal adhesives are class 1 carcinogens (Altowayti et al., 2021; Li et al., 2021). Nickel is a heavy metal commonly found in wastewater derived from industries of coal, diesel, and fuel oil, and the incineration of waste and sewage. Overexposure to nickel can cause nausea, vomiting, diarrhea, headache, cough, and shortness of breath and up to death (Costa et al., 2022; Khadim et al., 2019). Other than heavy metals, organic pollutants like synthetic dyes are also among the most common pollutants that can be found in wastewater (Thirunavukkarasu et al., 2020). Global consumption of synthetic dyes is roughly 7×10^5 tons per year, of which the textile industry consumes about two-thirds. Consumption of synthetic dyes produces large volumes of wastewater discharged into aquatic ecosystems. For example, Congo red (CR), is a known carcinogenic compound that produces toxic effects in the hydrations, reduces light penetration, and alters the photosynthetic activity, causing oxygen depletion, among other effects in water bodies (Akhtar et al., 2020; Hernández-Zamora and Martínez-Jerónimo, 2019). Moreover, the textile industry wastewater has emerged as a pressing environmental concern due to its composition, which includes organic dyes, suspended solids, dissolved solids, and heavy metals. When synthetic textiles are used and discarded, they release microfibers into the environment, often measuring less than 5 mm (and sometimes as small as 1 mm). Furthermore, microplastics—resulting from the degradation of larger plastic items—pose a real threat by potentially fouling membranes. Although coagulation/flocculation processes serve as pretreatment measures to prevent fouling, some pollutants still manage to evade these processes. Consequently, efficient treatment options like membrane filtration play a crucial role in addressing this issue (Aragaw and Bogale, 2023; Ramasamy et al., 2022).

Other common pollutants found in wastewater include suspended particles like sand, personal care products, plastic additives, anticorrosives, flame retardants, detergents, chemicals excreted from urine and feces, pesticides, hydrocarbons, and biological pollutants like bacteria, viruses, and fungi (Madeira and de Araújo, 2021). This pollutant deposition in the water bodies needs to be controlled and eliminated to improve environmental safety.

The current wastewater treatment techniques can be categorized into three classes such as physical, chemical, and biological methods (Ashraf et al., 2021). Physical methods include techniques like sedimentation and membrane separation. These techniques are characterized by physical activity resulting in the elimination of the non-dissolved pollutants in the wastewater. This method is suitable for the removal of biological pollutants like bacteria, viruses, fungi, and suspended particles (Ali, 2012; Zhang et al., 2016). However, the removal of dissolved pollutants is ineffective in the physical approach (Barman et al., 2021). Chemical methods include techniques such as precipitation, coagulation, ion exchange, adsorption, neutralization, and solvent extraction. The main advantage of this approach is the removal of targetted, dissolved, and a wide pollutant spectrum. However, the approaches often involve complex reaction that creates requirements for secondary treatment (Ahmad et al., 2015; Tang et al., 2016). Biological methods are suited mostly for very large-scale wastewater treatment however lack flexibility in operation (Meena et al., 2019). While the current wastewater treatment approaches can remove conventional pollutants like suspended particles, clays, bacteria, and other microorganisms, to eliminate the wider pollutants from the wastewater, it is necessary to develop a hybrid system that combines multiple mechanisms (Dhangar and Kumar, 2020). Emerging approaches such as electrocoagulation are also being studied as effective wastewater treatment methods. Electrocoagulation combines coagulation, flotation, sedimentation, and electrochemistry. It outperforms traditional approaches due to its simplicity, reduced sludge production, low maintenance requirements, and cost-effectiveness. Specifically suited for oil-containing wastewater, electrocoagulation is promising. However, as a relatively new process, it requires further research to optimize its overall performance and address any limitations such as high dependence on parameters such as pH, electrode material and configuration, oil concentration, electrolyte concentration, etc. (Kadier et al., 2022; Al-Qodah et al., 2024). Another approach involves combining hybrid materials by pairing. One such pairing involves metal-organic frameworks (MOFs) with naturally occurring hierarchical diatom biosilica. The adsorbent has yielded promising results, including 99.02 $\pm$ 1.3% degradation efficiency against malachite green (MG) and efficient removal of Pb^{2+} ions (96.45 $\pm$ 2.1% removal efficiency). However, the degradation process was carried out in 60 min, and the outcomes for a wider range of dyes varied from 75% to 98%, indicating both potential and room for improvement (Uthappa et al., 2020). Another avenue explored the extraction of Casein, a protein-based biopolymer derived from cow's milk. Casein exhibited electrostatic interactions, hydrogen bonding, hydrophobic interactions, and π-π interactions, highlighting its potential as a biobased green material. Nevertheless, its performance across a broader spectrum of dyes remained between 70% and 85%, suggesting promising results but still leaving space for enhancement (Hegde et al., 2024).

This paper describes the synthesis of a highly efficient green ternary nanocomposite for wastewater treatment. The approach combines adsorption and size exclusion mechanisms to remove pollutants. The nanocomposite formulations include biomass-derived nanocellulose (NC), chitosan (CH), and calcium phosphate (CaP). Nanocellulose, abundant in nature, provides a fibrous matrix for filtration-based structures due to its toughness and linearity (Deepu A Gopakumar et al., 2019a; Peter et al., 2022). Chitosan, another natural polysaccharide, exhibits strong adsorption capacity for anionic and cationic dyes, and heavy metal ions, and acts as an anti-bacterial agent (Peter et al., 2020; Zhu et al., 2010). Calcium phosphate, an environmentally friendly material, effectively adsorbs heavy metals, dyes, and organic pollutants (Lyczko et al., 2014a, 2017). Additionally, it imparts mechanical properties to the membrane. By combining these socially and environmentally friendly materials, the nanocomposite addresses key challenges in wastewater treatment, targeting dissolved pollutants and larger particles. The wastewater used in this study was collected from the wastewater treatment plants in Graulhet, France. These treatment plants handle wastewater from households, hospitals, and industries. Before filtration, the wastewater was centrifuged at 20,000 rpm for 10 min to remove suspended particles. The wastewater was collected before the buffering step to avoid any sewage stabilization that could change the polluted water characteristics (Zhang et al., 2016). Table 1 presents recent research on wastewater treatment applications. While efforts

have been made to enhance filtration membrane performance as evident from the works cited, many of these studies rely on toxic chemicals, complex procedures, and expensive materials, leading to high capital and operational costs. We have opted for striking a balance between cost-effectiveness and eco-friendliness while not compromising on performance. This approach also aligns with the UN's sustainability goals.

2. Materials and methods

2.1. Materials

Calcium phosphate powder (CaP) is provided by PRAYON. The nanocellulose suspension (NC) and chitosan powder (CH) were purchased from a Canadian-based NC supplier named Cellulose Lab. The chitosan powder was in powder form with 90% deacetylation and was commercialized by the name Chitosan. The Chitosan was used as chitosan powder (Po-CH) and as dissolved chitosan (Dis-CH) where 1 g of chitosan powder was dissolved in 1 wt% acetic acid solution (100 ml) to obtain a concentration of 1 wt% of dissolved chitosan (Thomas et al., 2016).

2.2. Ternary nanocomposite fabrication

The fabrication of ternary nanocomposite was done following an already reported vacuum filtration method with modification (Lin et al., 2021). The components were introduced into a standard flask of 250 ml volume (CaP and Po-CH), NC suspension (3 wt% NC), and solution (Dis-CH = 1 wt % of chitosan powder). After collecting each component in specified quantities, distilled water was added. The concentration of nanocellulose (X) and calcium phosphate (1.5×) has been kept constant. The samples used in the studies are: NC: CaP, NC: CaP: Po-CH (0.25×), NC: CaP: Dis-CH (0.1×), NC: CaP: Dis-CH (0.15×). The components were introduced into the water were homogenized at room temperature using a homogenizer (IKA T 25 digital Ultra-Turrax) at 12,000 r.p.m. for 15 min to ensure good dispersion. The homogenized suspension was immediately vacuum filtrated using a filtration setup followed by drying for 24 h under load at room temperature as shown in Fig. 1.

2.3. Characterization methods

The morphology of the nanocomposites was observed using a Philips XL 30 ESEM FEG with an accelerating voltage of 15 kV. The local chemical formulations at a micro-scale were determined by using an energy-dispersive X-ray spectroscopy (EDX) module. Fourier Transform Infrared spectrophotometer Nicolet model IN10 MX Thermofisher was used. IR spectra of all samples from 500 to 4000cm-1 were measured. BET method (Brunauer, Emmett and Teller) was used to determine the specific surface areas and the porosity by Micromeritics BET Tristar II. HORIBA Jobin Yvon Ultima 2 inductively coupled plasma mass spectrometer (ICP-MS) was used for the elemental analysis of heavy metals. The Congo red analysis was carried out with HP 8452 UV-VIS Spectrophotometer within the 400 nm–700 nm range where 498 nm was used as the identification peak.

The flexibility test was carried out on a nanocomposite sample flexed up to 100 times with a nip gap of 20 mm distance. After the 100 cycles of flexing, the unbroken samples were tensile tested using equation (1.1).

The tensile breaking test where a preload of 2 kN to the sample was later applied at a strain rate of 5 mm/min.

$$\text{Tensile strength } \sigma_{max} = P_{max}/A_0 \quad 1.1$$

where tensile strength (kN/cm^2), P_{max} = maximum load (kN), A_0 = original cross-sectional area (cm^2).

2.4. Pollutants removal experiments

Pollutant (heavy metals and Congo red dye) removal experiments were conducted in a stirred cell filtration system (SterlitechTM HP4750, USA) (Lin et al., 2020). In the beginning, the nanocomposite membrane was wetted by dipping it in deionized water for 15 min. This procedure was used to prevent membrane compaction throughout the permeation or separation experiments. The temperature of the feed solution and pressure were maintained at room temperature (25 °C) and 10 bar (Selected from literature studies).

The quantity of the pollutants removed was calculated from the following equation:

$$\text{Pollutant removal percentage} = \left(\frac{C_i - C_t}{C_i}\right) x100 \quad 1.2$$

where C_i and C_t are the pollutant ions concentrations in mg/L at the beginning of the experiment and as a function of time t in min with lower detection limit of 10 ppb.

3. Results and discussions

Morphological characterization was used to observe the interactions

Table 1
Comparison of our work with recent similar works.

Materials	Fabrication technology	Claims	Advantage of our work	Reference
Oleic acid, carbon nanotubes, Polyvinylidene fluoride	Vacuum filtration	High salt rejection (99.45%) high water flux (89 LMH) 30% higher than unmodified PTFE membrane	No sample preparation No use of fluoropolymers Careful selection of adsorbent instead of modification Green membrane	Pouya et al. (2021)
Two-dimensional graphene oxide (GO), phosphomolybdic acid	multi-step process assisted with hydrothermal treatment	water permeance of ~275 ± 10 L m^{-2} h^{-1} separation efficiency (~99%) for salts	Simple process Low cost Greener approach Scalability	Soomro et al. (2023)
Polysulfone (PSF), dimethylacetamide (DMA), polyvinylpyrrolidone (PVP)	Solution casting	Flux recovery ratio (95.8%), Reactive Green 19 dye rejection (99.6%), and tensile strengths of the PEI-SiO2/PSF membranes over the neat PSF and SiO2/PSF membranes	Green membrane Cost-effectiveness Non-toxic chemical use	Vatanpour et al. (2022)
Polyvinyl alcohol, polyethersulfone, carbon nanotubes, graphene oxide	Phase inversion	Carbon nanotube and graphene oxide membrane showed 54 % and 35 % higher flux compared to neat polyethersulfone	Simpler process Cost-effective High flow Obtained via optimization Green membrane	Behdarvand et al. (2021)
Piperazine (PIP), noria, polyamide layer, glutaraldehyde	Condensation reaction	Na_2SO_4 rejection (~98%) and 147.6 L m^{-2}h^{-1}MPa^{-1} of water permeability	Simpler process Cost-effective Green approach	Yang et al. (2021)

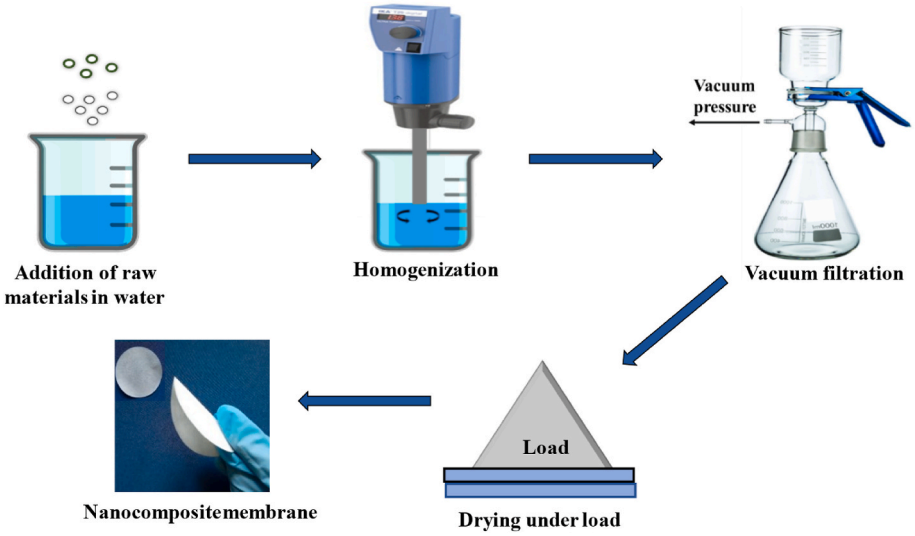

Fig. 1. Schematic representation of the nanocomposite preparation.

between raw materials in the nanocomposite which was also qualitatively evaluated and conclusive observations were made using FTIR analysis. Fig. 2(a) presents the internal morphological structures NC: CaP where nanocellulose (yellow arrow) and calcium phosphate (blue arrow) can be seen. The CaPs appear as agglomerated particles in different shapes and sizes based on the agglomerations. The nanocellulose appears in fiber-like shapes and entrapping the calcium phosphate particles. Fig. 2(b) shows a magnified image of a portion presented in Fig. 2(a), here the calcium phosphate particles are entrapped and deposited over the nanocellulose structures can be observed. This indicates there is an interaction between the components in the nanocomposite. Moreover, various pores/spaces created between CaP and nanocellulose can be observed. These inter and intra-particle spaces can potentially play an important role in pollutant entrapment. Fig. 2(c) and (d) correspond to the SEM and EDX images of the nanocomposite namely NC: CaP at 100 μm of magnification. The non-uniformity (heterogeneity) in the surface of the green nanocomposite membrane derived from the agglomerated calcium phosphate (CaP) particles can be observed. EDX analysis was made in a portion (Fig. 2(c), red box), the presence of calcium phosphate on the surface of the composite can be observed from the peaks of Ca, P. The presence of nanocellulose is evidenced by the peaks of C, and O. The different images demonstrated that the green ternary nanocomposite is a flexible material that has nanocellulose as the main matrix. Fig. 2(e) illustrates the FTIR spectrographic image of the nanocomposite where peaks of 3424 cm^{-1} are attributed to the OH stretching vibration, 2921 cm^{-1} corresponds to the C–H asymmetric and symmetric tensile vibration in the pyranoid ring. The peak at 1636 cm^{-1} originates from the bending mode of the absorbed water. The band at 1372 cm^{-1} is due to the OH bending vibration. For NC specifically, the absorption peaks at 1433 cm^{-1}, 1164 cm^{-1}, 1114 cm^{-1}, 1058 cm^{-1} and 896 cm^{-1} relate to the CH^2 symmetric scissoring in the pyranoid ring, C–O antisymmetric bridge stretching, the crystal absorption peak of cellulose I, C–O–C pyranoid ring skeletal vibration and the -glycosidic linkages. In the case of CH specifically, intensities of the ($CO–NH_2$) band at 1641 cm^{-1} and the (NH_2) band at 1598 cm^{-1} are observed. Whereas for CaP, peaks at 1038 cm^{-1}, attributed to the PO_4^{3-} respectively were observed in the nanocomposite demonstrating the wide range of functional groups that are present in the nanocomposite as predicted (Malik et al., 2020). Based on the SEM results, the non-uniform surface resulting from agglomerated calcium phosphate (CaP) particles impacts the filtration efficiency of the green ternary nanocomposite membrane. These irregularities create additional surface area, enhancing adsorption and particle entrapment. Additionally, the FTIR analysis reveals critical functional groups, such as OH stretching vibration, C–H tensile vibration, and the presence of NC, CaP, and CH. Overall, these observations contribute to the nanocomposite's potential adsorption capacity, mechanical properties, and effectiveness in wastewater treatment.

The physical properties of the raw materials and nanocomposites are presented in Table 2. Owing to the higher surface area and pore characteristics of calcium phosphate (CaP), these features were also evident in the nanocomposite, particularly in the isotherm. All the samples exhibited a type IV isotherm as specified by IUPAC, with mesopores. This information is important, as it indicates that the nanocomposites exhibit multiple surface layer formation (Gotor et al., 2000; Hameed et al., 2008). The nanocomposite NC: CaP exhibited the highest physical properties (surface area, pore volume, and pore diameter), this was followed by NC: CaP: Dis-CH (0.1×), NC: CaP: Po-CH (0.25×) and NC: CaP: Dis-CH (0.15×). The pore diameter values show that the nanocomposites have mesoporous structures (2 nm < d_{pore}< 50 nm) and pore diameter values similar to calcium phosphate. To understand the physical characteristics of the nanocomposite, the characteristics of the raw materials have to be compared and evaluated. The calcium phosphate used in the study has a surface area of 87.5 m^2/g, pore volume of 0.4 cm^3/g, and pore diameter of 20.7 nm. Whereas the nanocellulose has a surface area of 11.7 m^2/g, chitosan has a surface area of 7.8 m^2/g and 2.9 m^2/g for powder form and film form respectively. This was directly reflected in the physical characteristics of the nanocomposites. For instance, NC: CaP nanocomposite exhibited the highest surface area of 53.9 m^2/g in comparison with the other nanocomposites that included chitosan. The incorporation of calcium phosphate increases the surface area and pore characteristics and chitosan reduces the surface area and pore characteristics of the nanocomposites (Fu et al., 2008; Park et al., 2007). Szatkowski et al. (2015)reported a similar influence in a composite fabricated with calcium hydroxyapatite and chitosan in a one-step process. The surface area of pure hydroxyapatite was 80 m^2/g, and the pore volume was 0.4 cm^3/g. In comparing different composite formulations, the highest surface area (81.0 m^2/g) was found for the sample containing the highest amount of hydroxyapatite and lowest chitosan in formulation (HAP/CS:85/15), whereas the lowest surface area (23.0 m^2/g) was found for the formulation HAP/CS:70/30 sample (Yanti and Pebrianti, 2021). The nanocomposite formulation, which includes biomass-derived nanocellulose (NC), chitosan (CH), and calcium phosphate (CaP), exhibits mesoporous structures with pore diameters between 2 nm and 50 nm. Notably, the NC: CaP nanocomposite demonstrates the highest surface area, pore volume, and pore diameter.

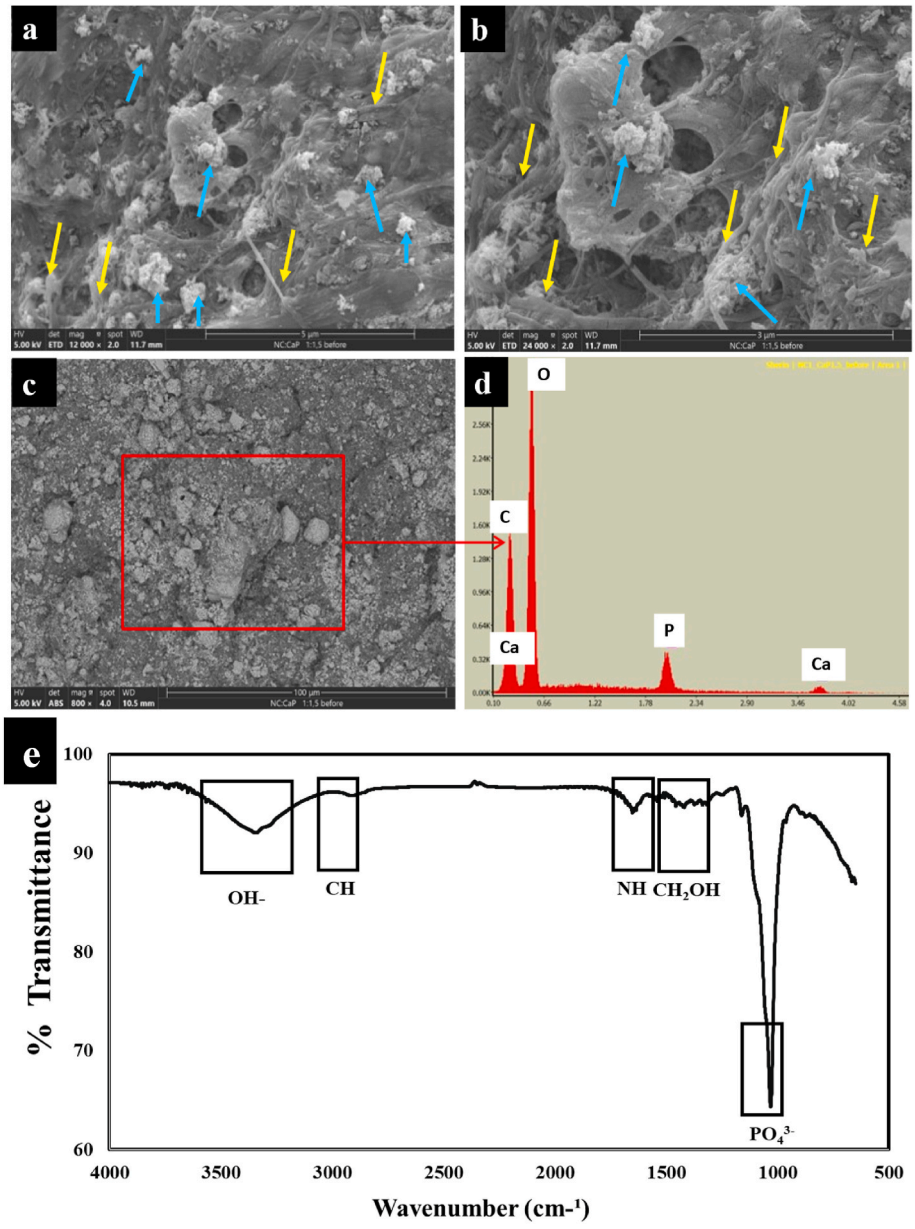

Fig. 2. Nanocomposite NC: CaP: Po-CH (0.25×) a) SEM image at 5 μm (b) SEM image at 3 μm (c & d) SEM-EDX of selected areas in figure c (e) FTIR graph.

Table 2
Surface area and porosities of green nanocomposites.

Nanocomposites	Surface area S_{BET} (m^2/g)	Pore volume V_{pore} (cm^3/g)	Pore diameter dp (nm)	Isotherm (IUPAC)
CaP Powder	87.5	0.4	20.7	Type IV with mesopores
NC film	11.7	–	–	
Chitosan film	2.9	–	–	
Chitosan powder	7.8	–	–	
NC: CaP	53.9	0.2	18.7	
NC: CaP: Dis-CH (0.1×)	46.3	0.2	20.0	
NC: CaP: Dis-CH (0.15×)	39.2	0.2	20.4	
NC: CaP: Po-CH (0.25×)	40.9	0.2	18.6	

Comparing raw materials, CaP contributes to increased surface area and pore characteristics, while chitosan reduces them. These insights are essential for optimizing nanocomposite design and enhancing their effectiveness in treating wastewater.

The productivity of the nanocomposite depends on the flux rate, which was investigated using a dead-end filtration cell. The flux rate of the different nanocomposites is presented in Fig. 3(a). The difference in the flux rate in comparison to NC: CaP: Dis-CH (0.15×) is provided in the bracket since it had the lowest flux rate. The NC: CaP: Po-CH (0.25×) (145%) has the highest flux rate of 146 L/m^2.h.MPa. This was followed by NC: CaP (115%) with 30% difference in flux rate of 125 L/m^2.h.MPa. However the NC: CaP: Dis-CH (0.1×) (29%) and NC: CaP: Dis-CH (0.15×) have flux rates of 78 L/m^2.h.MPa and 58 L/m^2.h.MPa respectively. The incorporation of dissolved chitosan reduced the flux rates and it can be explained by the fiber-thickening effect of dissolved chitosan where the chitosan polymer chain adheres to the cellulose nanofibers and calcium phosphate particles resulting in reduced flow channel diameter (Ilyas et al., 2022; Nechyporchuk et al., 2020) Moreover, the incorporation of powder chitosan increased the flux rates since the

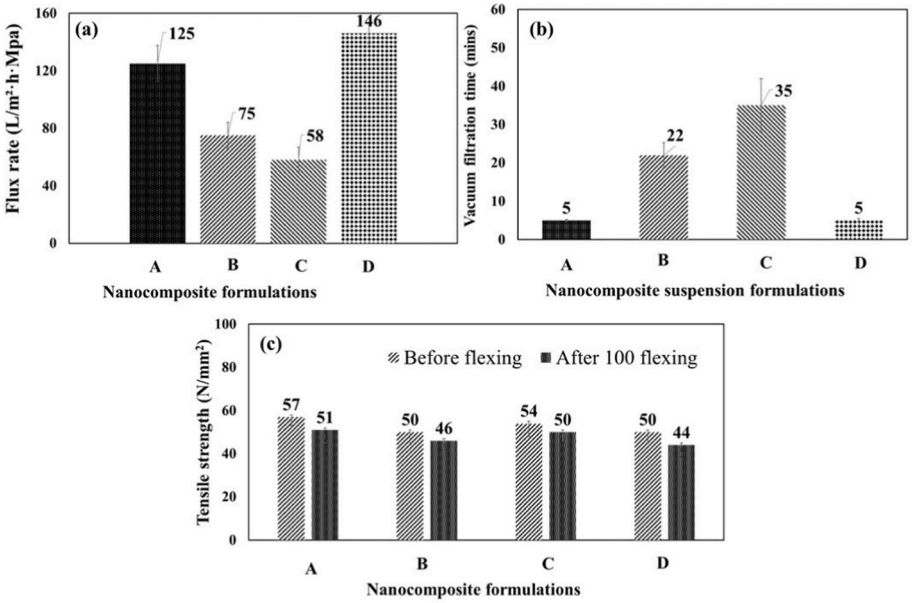

Fig. 3. Different physical characterization graphs:(a) Operating time (b) Vacuum filtration time and (c) Mechanical performance where A: NC: CaP, B: NC: CaP: Po-CH (0.25×), NC: CaP: Dis-CH (0.1×), NC: CaP: Dis-CH (0.15×).

incorporation of powder forms increases the heterogeneity of the nanocomposite. The influence of increasing heterogeneity in reducing filtration time has been reported in other studies ("Effect of Process Related Factors on Filtration Rate - Labmonk," n. d.; Jiang, 2003). These insights are essential for optimizing nanocomposite design and enhancing their operating time in treating wastewater.

Vacuum filtration time during the fabrication of the nanocomposite has a direct correlation with the productivity of the nanocomposite. The vacuum filtration time presented in Fig. 3(b) shows that the nanocomposite that does not include dissolved chitosan has a faster vacuum filtration time of 5 min for both NC: CaP: Po-CH (0.25×) and NC: CaP. The vacuum filtration time for the other two nanocomposites that were synthesized with dissolved chitosan followed the order of NC: CaP: Dis-CH (0.1×) > NC: CaP: Po-CH (0.25×) where the vacuum filtration times are 22 and 35 min respectively. On comparing the vacuum filtration time of the different nanocomposites, the maximum vacuum filtration time was taken by NC: CaP: Dis-CH (0.15×) (35 min) compared with the NC: CaP (5 min). Whereas for the nanocomposites with dissolved chitosan incorporation, with a 50% reduction of dissolved chitosan in the composition, a 37% reduction in vacuum filtration time was observed (between NC: CaP: Dis-CH (0.15×) and NC: CaP: Dis-CH (0.1×)). The incorporation of dissolved chitosan significantly increases the vacuum filtration time. This could be due to the thickening nature of the dissolved chitosan where the dissolution results in an increase of the suspension viscosity as well as deposition over the nanocellulose fibers resulting in reduced flow channels that increase the vacuum filtration time (Jamshidifard et al., 2019a; Weiβpflog et al., 2021). These insights are essential for optimizing nanocomposite design and enhancing the fabrication of the nanocomposite. Because the understanding of these dynamics guides nanocomposite fabrication for optimal performance and fabrication.

Mechanical testing was employed to evaluate the internal microstructural integrity of the synthesized nanocomposites. Fig. 3(c) corresponds to the tensile strength of the nanocomposites before and after 100 cycles of the flexing test (the difference is provided in the bracket). This approach of comparing the tensile strength before and after flexing enabled the evaluation of the flexibility as well as the strength of the nanocomposites. The nanocomposite NC: CaP (10.5%) exhibited the highest mechanical strength values. This was followed by NC: CaP: Dis-CH (0.1×) (7%) and NC: CaP: Po-CH (0.25×) (8%). The nanocomposite NC: CaP: Dis-CH (0.1×) (12%) exhibited the lowest mechanical strengths. Increasing the calcium phosphate and chitosan concentration introduced into the nanocellulose-based matrix resulted in the reduction of mechanical strength. This could be due to the hindrance caused by the incorporated particles to the nanocellulose fibers from forming a strong film. Hence, an increment in the quantity of the incorporated particles results in the reduction of mechanical performance proportionally (Shim et al., 2007; Zhao et al., 2019). In summary, understanding these relationships guides nanocomposite design for optimal performance in membrane fabrication. These insights guide the composition of components in the nanocomposite to enhance their effectiveness in treating wastewater.

The performance of the synthesized nanocomposite membrane in filtration studies demonstrated that the synthesized nanocomposite exhibits sufficient mechanical characteristics (flexibility of above 100 cycles and tensile strength of about 50 N/mm^2). The nanocomposite exhibited tensile strength values between 50 and 57 N/mm^2 which are comparable to the literature values between 5 and 60 N/mm^2 (Weng et al., 2017; Zhu et al., 2015). Similarly, the flow rate and filtration studies also indicate that the nanocomposite can be synthesized in a very short time (up to 5 min) and operated in a short time (up to 21 min). Moreover, the influences of the different concentrations of raw materials in the formulation have also been recognized as a function of the nanocomposite membrane performance outcomes.

3.1. Pollutant removal studies from synthetic solutions and mechanism

The work examined the removal of pollutants in synthetic wastewater, specifically Ni ions and Congo red dye, using different nanocomposites and various concentrations of Ni ions and CR dyes mixed. The results are presented in Fig. 4(a) and (b), with the values in brackets. In Fig. 4(a), it can be seen that at a concentration of 10 ppm of Ni ions, the nanocomposite NC: CaP: Dis-CH (0.1×) achieved the highest pollutant removal of 98.7%. The nanocomposites NC: CaP: Dis-CH (0.15×) (98.4%) and NC: CaP: Po-CH (0.25×) (98.2%) showed similar pollutant removal values, while NC: CaP (95.8%) had the lowest removal values. At 50 ppm, the order of pollutant removal remained the same as at 10 ppm. However, the removal percentage decreased by 3% for all nanocomposites. As the pollutant concentration increased to 100 ppm and 150 ppm, the order of maximum pollution removal by

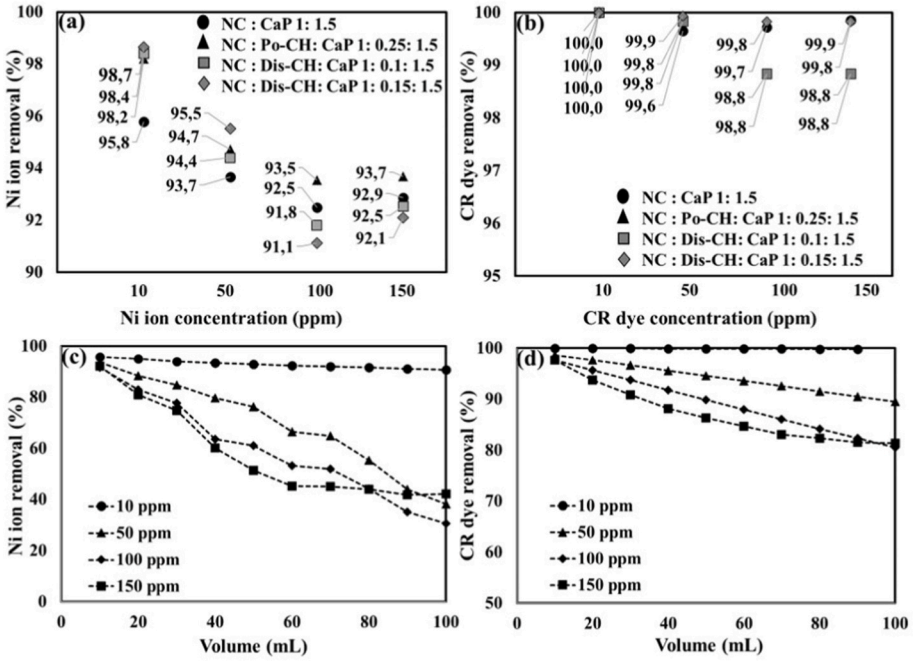

Fig. 4. Pollutants removal using different nanocomposites (a) Ni ions and (b) CR dye, (c) Ni ion removal using NC: CaP at (10, 50, 100 and 150 ppm), (d) CR dye removal using NC: CaP at (10, 50, 100 and 150 ppm).

nanocomposites changed. The nanocomposite NC: CaP: Dis-CH (0.1×) (93.5%) exhibited the highest percentage of pollutant removal, followed by NC: CaP: Dis-CH (0.15×) with 92.5%. NC: CaP: Dis-CH (0.1×) and NC: CaP: Dis-CH (0.15×) had pollutant removal percentages of 91.8% and 91.5% respectively. For the synthetic solution of CR dye with a concentration of 10 ppm, all four nanocomposites completely removed the dye (Fig. 4(b)). A similar trend to the Ni ion removal was observed for the synthetic solutions of CR dye with concentrations of 50 ppm, 100 ppm, and 150 ppm.

Three significant findings have emerged from the research on pollutant removal using synthetic polluted solutions. The initial discovery is the notable disparity in the removal rates of CR dye and Ni ions at varying pollutant concentrations. The larger particle size of CR dye molecules (2.7 nm in length) compared to Ni ions (0.065 nm or 0.085 nm in diameter) likely explains the preference for a filtration-based approach to removing pollutants (Ueno et al., 1983; Wanyonyi et al., 2014). Furthermore, the diverse surface groups present in the nanocomposite, such as Ca^{2+}, NH^{3+}, OH-, and PO_4^{3-}, interact more effectively with CR dye (due to the presence of various functional groups like NH_2^+, SO^{3-}, and Na^+) than with Ni^{2+}, which consists of only a single atom (Gopi et al., 2019; Pasquini et al., n.d.). Another observation pertains to the maximum pollutant removal percentage between 10 ppm and 50 ppm is attributed to the physical characteristics of the nanocomposites. At lower pollutant concentrations, the nanocomposite interacts more efficiently with the pollutants due to the slower saturation of surface functional groups (Huang et al., 2012; Jamshidifard et al., 2019b). Additionally, the smaller pore size (pore volume and diameter) facilitates better entrapment through size exclusion. This is evident in the ranking of nanocomposites based on pollutant removal percentage, with NC: CaP: Dis-CH (0.1×) and NC: CaP: Dis-CH (0.15×) demonstrating superior removal rates compared to NC: CaP. The third observation involves the shift in the ranking of nanocomposites based on pollutant removal percentage at concentrations of 100 ppm and 150 ppm. As the concentration of pollutants in the synthetic solutions increases, the surface functional groups saturate more rapidly, leading to more efficient pollutant removal by nanocomposites with superior physical properties (Ma et al., 2000).

The pollutants removal (both CR dye and Ni ions) was further investigated using scanning electron micrography coupled with energy-dispersive X-ray spectroscopy to compare the morphological and elemental composition before and after filtration experiments to understand the mechanism. The NC: CaP: Po-CH (0.25×) nanocomposite with 50 ppm concentration of both CR dye and Ni ion in the synthetic solution was characterized as shown in Fig. 5. On evaluating the SEM images, Fig. 5(a), shows calcium phosphate are in agglomerated in the nanocomposite. The corresponding EDX (Fig. 5(b) shows the Ca and P peaks which are characteristics of calcium phosphate along with C and O peaks which are characteristics of nanocellulose and chitosan. Fig. 5(c) and (d) present the SEM images and EDX of NC: CaP: Po-CH (0.25×) at 100 μm after filtration. From Fig. 5(c), the topography of the SEM image derived from the CR dye deposition appeared darker in comparison with Fig. 5(a). The EDX of Fig. 5(b) shows increased peaks of C, followed by O, and then new peaks of Ni, S, and P also appeared. The presence of Ni ions and S are characteristics of pollutants used in synthetic solutions. The deposition of Ni and CR dyes on the surface, as well as the reduction of oxygen and calcium, also indicates hydrogen bonding, surface complexation, and ion exchange reaction mechanisms (van Rijt et al., 2021). Another potential mechanism is electrostatic interactions since all the nanocomposite components are reported to exhibit surface charge.

The internal structure of the NC: CaP was examined by introducing a transverse cut into the nanocomposites as shown in Fig. 6. Fig. 6(a) shows the difference between both the internal structure and external surface to which pollutants were introduced. Fig. 6(b) presents the magnified image of the top surface where the deposition of pollutants can be observed in the marked areas (red square). In Fig. 6(c), the internal structure of the nanocomposite can be observed. The yellow arrows point toward the agglomerated calcium phosphate particles and the blue lines point toward the fibrilar network formed by nanocellulose fiber. This image does not present any characteristic patterns of CR dye which is evident in Fig. 6(b), (d), and 6(f). Fig. 6(f) presents the 1 μm magnified image of the portion indicated in Fig. 6(d). The image shows the thick and agglomerated deposition of a chip-like structure indicative of CR dye pollutants on the surface of the nanocomposite. This particular image indicated that the main pollutant removal mechanism involved in the process is size exclusion. The bigger CR dye molecules were mostly

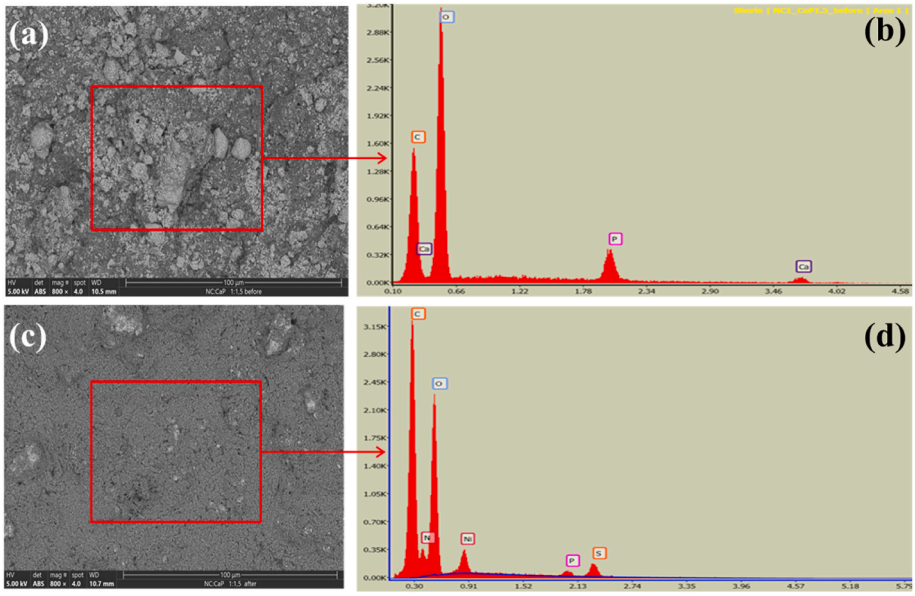

Fig. 5. NC: CaP: Po-CH (0.25×) top surfaces before filtration (a) SEM image (b) EDX. NC: CaP: Po-CH (0.25×) top surfaces after filtration (c) SEM image (d) EDX.

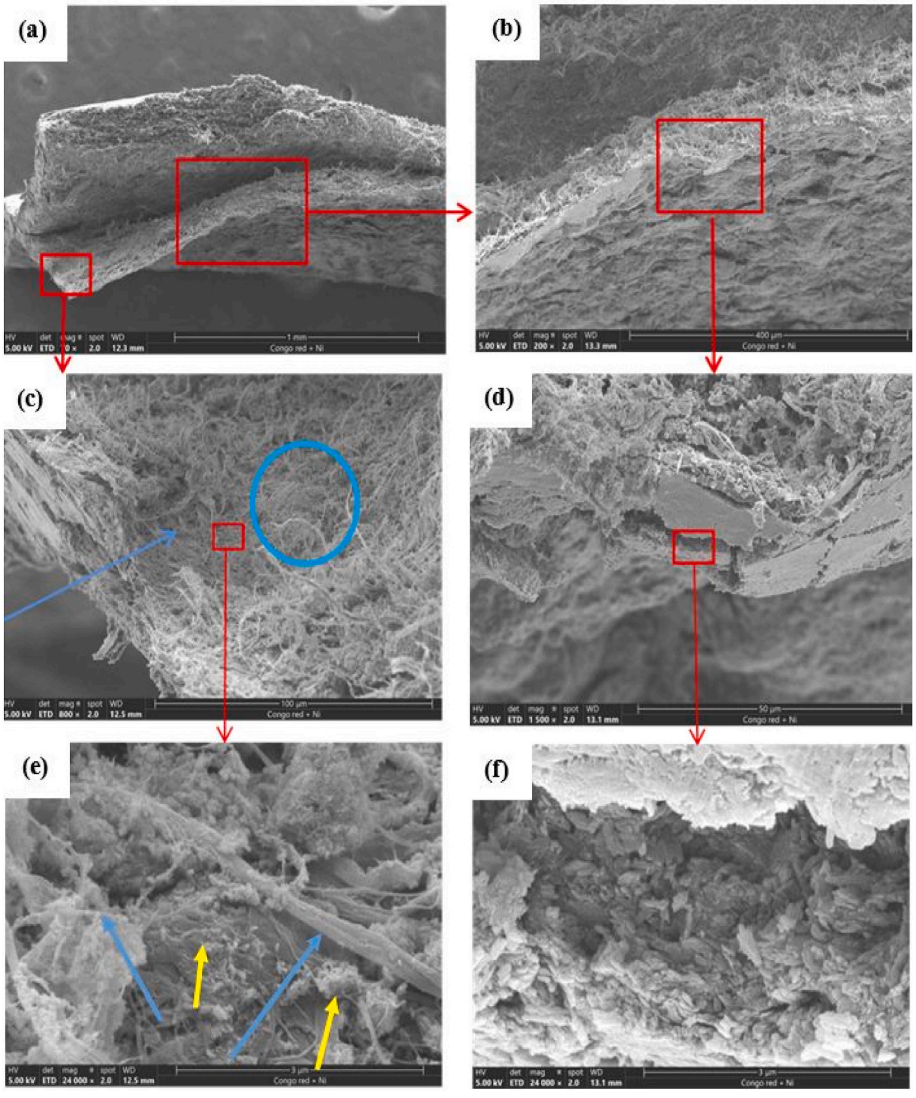

Fig. 6. SEM images of NC: CaP top and inside images after filtration.

excluded by size exclusion resulting in a thick layer formation with CR dye on the surface to which the synthetic solution was introduced. Moreover, the cross-section images (Fig. 6(c) and (e) do not show any morphological features of CR dye particles. Since the Ni ions cannot de size excluded and identified by the SEM analysis, the removal could be a function of various physical and chemical mechanisms.

The results indicate that there are various mechanisms involved in pollutant removal. The hybrid membrane pollutants removal mechanism involves a combination of filtration and sorption processes, where the nano cellulose membrane filters out larger pollutants (greater than 20 nm) while active sites are utilized to eliminate dissolved or smaller pollutants. Different mechanisms, either single or multiple, can impact the efficiency of pollutant removal. The initial phase involves the movement of pollutants from the feed bulk to the membrane interface (size exclusion), followed by the diffusion of pollutants through the membrane and into the pores or active sites. The predominant mechanisms driving this diffusion phase may include electrostatic interaction, ion exchange, surface complexation, and hydrogen bonding, which are characteristics of the material used in the nanocomposite synthesis (Hokkanen et al., 2016; Zhang and Wang, 2015). In summary, the mechanism of pollutants diffusion can be outlined as:

3.1.1. Congo red dye removal

The main removal mechanism is size exclusion because of its size (2.1 nm) and SEM-EDX has also proven higher deposition on the surface compared to inside (Fig. 6). The electrostatic interaction and hydrogen bonding (Hou et al., 2012).

Strong electrostatic interaction between positively charged sorbent surface and negatively charged CR dye

$$\equiv HPO_4Ca^{2+} + -O_6S_2C_{32}H_{22}N_6Na_2 \rightarrow \equiv HPO_4Ca^{+} \text{————} ^{-}O_6S_2C_{32}H_{22}N_6Na_2$$

$$\text{-}NH_3^{+} + -O_6S_2C_{32}H_{22}N_6Na_2 + H_2O \rightarrow (RNH_2)^{+}{}_n \text{————} ^{-}O_6S_2C_{32}H_{22}N_6Na_2 + OH\text{-}$$

Hydrogen bonding between hydroxyl groups and the pollutant (Here R can be CaP, CH or NC)

$$R\text{–}OH\text{–} + O_6H_{22}S_2C_{32}H_{22}N_6Na_2 \rightarrow nR\text{—}OH\ O_6H_{22}S_2C_{32}H_{22}N_6Na_2$$

3.1.2. Ni ion removal

The Ni ion removal mechanism can be surface complexation, electrostatic interaction, and ion exchange.

Surface complexation between the sorbent and Ni ion:

$$\equiv CaOH_2^{+} + Ni^{2+} \rightarrow \equiv CaOHNi^{+}$$

$$\equiv OP_2H^{-} + Ni^{2+} \rightarrow \equiv OPO_3Ni^{+} + H^{+}$$

Electrostatic interaction between positively charged sorbent surface hydroxyl group and Ni ion

$$\equiv CaOH + 2H_3O^{+} + Ni^{2+} \rightarrow \equiv CaOH^{-} \text{————} Ni^{+} + 2H_2O$$

$$R\text{–}OH\text{–} + Ni^{2+} \rightarrow R\text{-}O^{-} \text{————} Ni^{2+}$$

The ion-exchange reaction between positively charged sorbent surface and Ni ion

$$\equiv Ca_{10}(PO_4)_6(OH)_2 + Ni^{2+} \rightarrow \equiv (Ca_9)Ni(PO_4)_6(OH)_{2+}Ca^{2+}$$

$$\text{-}NH_3^{+} + Ni^{2+} \leftrightarrow R\text{–}NH_2\ \text{-}6\ Ni^{2+} + H^{+}$$

3.2. Pollutant removal from municipal wastewater

The pollutant removal efficiency of the nanocomposite membrane using municipal wastewater permeation experiments was conducted in a stirred cell filtration system. The identification and quantification of pollutants are presented in Table 3.

From the results shown in Fig. 7, the heavy metal Cd was removed completely (100%) from the wastewater (violet bars). The transition metals (black bars) such as Ag, Al, FE, Hg, Mo were completely removed whereas the Zn was removed 97%. The alkali earth metals such as Ba and Be were removed by 80 and 92% respectively. The alkali metal Li (green bar) was completely removed. The nonmetal (marron bars) P was removed 87% whereas the Se was removed completely. The nanocomposite membrane overall demonstrated a pollutant removal efficiency of 97% for all the elements in the wastewater. Moreover, it was observed that the pollutant removal was arbitrary. Multiple possibilities could be provided to explain the outcomes such as the complexity of pollutants that were removed, pore saturation, complexation and competition between the elements. From the literature, it was seen that the adsorption preference can be altered by both pollutants and the adsorbents (Mubarak et al., 2014). The ionic radius and ionic strength of pollutants could interact differently with different functional groups in the nanocomposite membrane (negatively charged groups like OH^{-}, PO_4^{3-} and positively charged groups like NH_2^{+}, Ca^{2+}). The surface complexation mechanism would also generate secondary complexes that can interact with pollutants leading to the pollutant's removal (Dabrowski et al., 2004; Qasem et al., 2021). Another possible mechanism is the pore saturation phenomenon, where the pollutants occupy the pores within the nanocomposite blocking the upcoming pollutants that can cause pore saturation. This mechanism was detailed in a study where Yurekli et al. (Yurekli, 2016) reported the mechanisms of adsorption in a multielement polluted system are related to the saturation membrane surfaces with the penetration of pollutants into pores. Based on the pollutant concentration of feed, the rate can be changed. That is, when the feed has a higher concentration of pollutants, the pore saturation can occur faster and the functional groups on the membrane can interact efficiently. Finally, the complexation occurring at the adsorption sites (top and borders of flow channels) within the nanocomposite causes increased hindrance since, in the case of NC: CaP nanocomposite, the raw materials like NC and CaP could perform multiple pollutant removal mechanisms such as surface complexation, electrostatic interaction, ion exchange (Deepu A. Gopakumar et al., 2019b; Gopi et al., 2019; Lyczko et al., 2014b). In summary, based on the results obtained, the nanocomposite could be used for the treatment of water in remote areas where the pollution concentration of heavy metals is a concern. Also, the green nanocomposite has performed outstandingly against Congo red dye indicating the potential of the nanocomposite to be used for the removal of dyes and organic pollutants. Moreover, the performance of the nanocomposite membrane is compared in Table 4 where the nanocomposites are made with unsustainable materials and complex techniques. However, the nanocomposite exhibited comparable and even superior pollutant removal capabilities.

Table 3
Pollutant concentrations found in the wastewater collected.

Elements		WWTP Concentrations (mg/L)
Heavy metals	Cd	0.30
Transition metals	Ag	0.52
	Al	0.08
	Fe	1.19
	Hg	1.6
	Mo	0.07
	Zn	0.45
Alkali earth metals	Ba	0.12
	Be	0.6
Alkali metal	Li	0.52
Non-metals	P	4.5
	Se	0.21

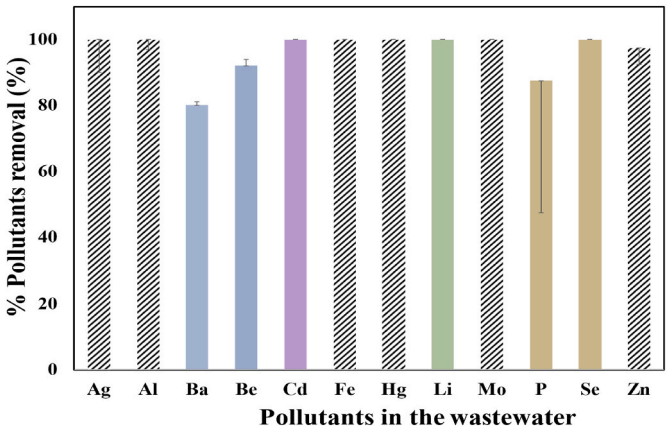

Fig. 7. Pollutant removal from industrial wastewater.

Table 4
Pollutant removal from different wastewater treatment studies.

Composite material	Pollutants removed	Initial pollutant concentration	Pollutant removal (%)	Reference
Halloysite nanotubes on polyvinylidene fluoride	Dyes and Heavy metals	100 ppm of Red 28, 5 ppm Cu^{2+}, Cd^{2+} and Cr^{6+} solution	94.9% for Red 28, Cu^{2+},Cd^{2+} and Cr^{6+} for M3 were 47.9%, 44.2% and 52.3%	Zeng et al. (2016)
Polyvinylidene fluoride (PVDF) membrane	Synthetic emulsified oily wastewater	Not specified	95% removal of organic contaminants	Wang et al. (2009)
Commercial polyvinylidene fluoride (PVDF) polymer	Inorganic materials	2500 mg/L and 5000 mg/L	75% of organic matter	Lateef et al. (2013)
PAN/MOF-808 membrane	Heavy metals	50 ppb	Zn^{2+} (54%) > Cd^{2+} (50%) > Pb^{2+} (46%) > Hg^{2+} (34%) Pb^{2+} ion 100% in mono-ion solutions	Efome et al. (2019)
polyacrylonitrile (PAN)/ polyaniline (PANI)-nylon core-shell nanofiber membrane	Heavy metals	50 mg/L	96.77% and 95.11% for Pb^{2+} and Cd^{2+}	Almasian et al. (2018)
Nanocellulose, chitosan and calcium phosphate	Dyes and Heavy metals, Industrial wastewater	10,50,100,150 ppm for both CR dye and Ni ion	97% for heavy metals and 100% for CR dye at 10 ppm. Upto 100% for multiple heavy metals	This work

4. Conclusions

This research aimed to create an environmentally friendly nanocomposite with exceptional pollutant removal capabilities in a simple method. By combining renewable resources (cellulose nanofibers and chitosan) with material calcium phosphate, we developed a ternary green nanocomposite. Notably, this formulation required no complex modifications or costly procedures. The nanocomposite operates at a very high flux rate of 146 L/m^2.h.MPa. Combines both adsorption (capturing heavy metals, dyes, and suspended particles) and size exclusion (selectively excluding contaminants based on size). In performance evaluations using synthetic and real-world wastewater, it achieved outstanding results: 100% removal of heavy metals like Cd, Ag, Al, Fe, Hg, Mo, Li, and Se, as well as significant removal rates for Ba, Be, P, and Zn. Importantly, its green synthesis approach avoids harmful chemicals. Looking ahead, exploring gradient-based strategies and scaling up for potable water production hold promise for practical applications. The main takeaways from the studies are as follows: The study demonstrated that a green ternary nanocomposite from renewable resources (cellulose nanofibers, chitosan) and material calcium phosphate without complex modification or expensive procedures. The green nanocomposite combines both adsorption and size exclusion that efficiently remove different heavy metals (proven based on real-world wastewater-based studies) and could be used to remove emerging pollutants.

However, this work also opens new questions and perspectives requiring further investigation. Open areas for future research include: The nanocomposite demonstrated impressive pollutant removal efficiency, achieving up to 98% removal of Ni ions and 100% removal of CR dye at lower pollution concentrations. Considering that natural water bodies typically have fewer pollutants than the synthetic polluted water used in this study, a remote drinking water solution could be proposed based on the results. The fabrication process is simple and requires minimal capital investment, making it an affordable and green option for remote areas facing water scarcity. Beyond wastewater treatment, the nanocomposite has potential for other applications. One avenue is pollutant recovery, where valuable materials trapped during the removal process could be reclaimed. Desorption experiments could efficiently recover elements that were inadvertently adsorbed by the nanocomposite. The nanocomposite's outstanding adsorption capacity for organic pollutants warrants further investigation. Specifically, studying its effectiveness in removing micropollutants such as dissolved antibiotics and hormones would be valuable due to its mesoporous structure.

In summary, this work not only provides a practical green solution for wastewater treatment but also opens doors for future research and applications in the field of green nanocomposites in various sectors.

CRediT authorship contribution statement

Sherin Peter: Writing – original draft, Project administration, Methodology, Investigation, Formal analysis, Conceptualization. **Nathalie Lyczko:** Writing – review & editing, Supervision, Project administration, Methodology, Investigation. **Sabu Thomas:** Writing – review & editing, Validation, Supervision, Project administration, Conceptualization. **Denis Leruth:** Writing – review & editing, Project administration, Funding acquisition, Conceptualization. **Alain Germeau:** Writing – review & editing, Project administration, Funding acquisition, Conceptualization. **Dorina Fati:** Writing – review & editing, Supervision, Resources, Project administration, Funding acquisition, Conceptualization. **Ange Nzihou:** Writing – review & editing, Validation, Supervision, Resources, Project administration, Methodology, Conceptualization.

Declaration of competing interest

The authors declare no competing interests.

Data availability

Data will be made available on request.

Acknowledgements

This work was financially supported by IMT Mines Albi of France and Prayon S.A. of Belgium.

Abbreviations

BET	Brunauer, Emmett and Teller
CaP	Calcium phosphate
CH	Chitosan
CNFs	Cellulose nanofiber
CR	Congo red
Dis-CH	Dissolved chitosan
EDX	Energy-dispersive x-ray spectroscopy
ICP-OES	Inductively coupled plasma optical emission spectrometer
MW	Molecular weight
NC	Nanocellulose
NFMs	Nanofiltration membranes
Po-CH	Chitosan powder
PVDF	Polyvinylidene fluride
SEM	Scanning electron microscopy
UN	United nations
XRD	X-ray diffraction

Appendix A. Supplementary data

Supplementary data to this article can be found online at https://doi.org/10.1016/j.chemosphere.2024.142779.

References

Ahmad, Mudasir, Ahmed, Shakeel, Swami, Babu, Ikram, Saiqa, 2015. Adsorption of heavy metal ions: Role of chitosan and cellulose for water treatment. Int. J. Pharmacogn. 2, 280–289. https://doi.org/10.13040/IJPSR.0975-8232.IJP.2(6).280-89.

Akhtar, A., Aslam, Z., Asghar, A., Bello, M.M., Raman, A.A.A., 2020. Electrocoagulation of Congo Red dye-containing wastewater: optimization of operational parameters and process mechanism. J. Environ. Chem. Eng. 8, 104055 https://doi.org/10.1016/J.JECE.2020.104055.

Ali, I., 2012. New generation adsorbents for water treatment. Chem. Rev. 112, 5073–5091. https://doi.org/10.1021/cr300133d.

Almasian, A., Giahi, M., Chizari Fard, G., Dehdast, S.A., Maleknia, L., 2018. Removal of heavy metal ions by modified PAN/PANI-nylon core-shell nanofibers membrane: filtration performance, antifouling and regeneration behavior. Chem. Eng. J. 351, 1166–1178. https://doi.org/10.1016/J.CEJ.2018.06.127.

Al-Qodah, Z., Al-Zghoul, T.M., Jamrah, A., 2024. The performance of pharmaceutical wastewater treatment system of electrocoagulation assisted adsorption using perforated electrodes to reduce passivation. Environ. Sci. Pollut. Control Ser. 31 https://doi.org/10.1007/s11356-024-32458-z.

Altowayti, W.A.H., Othman, N., Shahir, S., Alshalif, A.F., Al-Gheethi, A.A., AL-Towayti, F.A.H., Saleh, Z.M., Haris, S.A., 2021. Removal of arsenic from wastewater by using different technologies and adsorbents: a review. Int. J. Environ. Sci. Technol. 19 (9), 9243–9266. https://doi.org/10.1007/S13762-021-03660-0, 2021 19.

Aragaw, T.A., Bogale, F.M., 2023. Role of coagulation/flocculation as a pretreatment option to reduce colloidal/bio-colloidal fouling in tertiary filtration of textile wastewater: a review and future outlooks. Front. Environ. Sci. 11, 1142227 https://doi.org/10.3389/FENVS.2023.1142227/BIBTEX.

Ashraf, A., Ramamurthy, R., Rene, E.R., 2021. Wastewater treatment and resource recovery technologies in the brewery industry: current trends and emerging practices. Sustain. Energy Technol. Assessments 47, 101432. https://doi.org/10.1016/J.SETA.2021.101432.

Barman, S.R., Roy, U., Das, P., Mukhopadhayay, A., 2021. Membrane processes for removal of polyaromatic hydrocarbons from wastewater. Green Chemistry and Water Remediation: Research and Applications 189–207. https://doi.org/10.1016/B978-0-12-817742-6.00006-2.

Behdarvand, F., Valamohammadi, E., Tofighy, M.A., Mohammadi, T., 2021. Polyvinyl alcohol/polyethersulfone thin-film nanocomposite membranes with carbon nanomaterials incorporated in substrate for water treatment. J. Environ. Chem. Eng. 9 https://doi.org/10.1016/j.jece.2020.104650.

Costa, J.M., Costa, J.G. dos R. da, Almeida Neto, A.F. de, 2022. Techniques of nickel(II) removal from electroplating industry wastewater: overview and trends. J. Water Proc. Eng. 46, 102593 https://doi.org/10.1016/J.JWPE.2022.102593.

Dabrowski, A., Hubicki, Z., Podkościelny, P., Robens, E., 2004. Selective removal of the heavy metal ions from waters and industrial wastewaters by ion-exchange method. Chemosphere 56, 91–106. https://doi.org/10.1016/J.CHEMOSPHERE.2004.03.006.

Dhangar, K., Kumar, M., 2020. Tricks and tracks in removal of emerging contaminants from the wastewater through hybrid treatment systems: a review. Sci. Total Environ. 738 https://doi.org/10.1016/J.SCITOTENV.2020.140320.

Effect of Process Related Factors on Filtration Rate - Labmonk [WWW Document], n.d. URLhttps://labmonk.com/effect-of-process-related-factors-on-filtration-rate (accessed February.13.2022).

Efome, J.E., Rana, D., Matsuura, T., Lan, C.Q., 2019. Effects of operating parameters and coexisting ions on the efficiency of heavy metal ions removal by nano-fibrous metal-organic framework membrane filtration process. Sci. Total Environ. 674, 355–362. https://doi.org/10.1016/J.SCITOTENV.2019.04.187.

Fu, S.Y., Feng, X.Q., Lauke, B., Mai, Y.W., 2008. Effects of particle size, particle/matrix interface adhesion and particle loading on mechanical properties of particulate–polymer composites. Compos. B Eng. 39, 933–961. https://doi.org/10.1016/J.COMPOSITESB.2008.01.002.

Gopakumar, Deepu A., Arumughan, V., Beeran Pottathara, Y., S, S.K., Pasquini, D., Bračič, M., Seantier, B., Nzihou, A., Thomas, S., Rizal, S., Khalil, P.S., H, A., 2019a. Robust superhydrophobic cellulose nanofiber aerogel for multifunctional environmental applications. Polymers 11, 495. https://doi.org/10.3390/polym11030495.

Gopakumar, Deepu A., Arumughan, V., Pasquini, D., Leu, S.Y., Abdul Khalil, H.P.S., Thomas, S., 2019b. Nanocellulose-based membranes for water purification. Nanoscale Materials in Water Purification 59–85. https://doi.org/10.1016/B978-0-12-813926-4.00004-5.

Gopi, S., Pius, A., Kargl, R., Kleinschek, K.S., Thomas, S., 2019. Fabrication of cellulose acetate/chitosan blend films as efficient adsorbent for anionic water pollutants. Polym. Bull. https://doi.org/10.1007/s00289-018-2467-y.

Gotor, F.J., Criado, J.M., Malek, J., Koga, N., Gotor, F.J., Criado, J.M., Malek, J., Koga, N., 2000. Kinetic analysis of solid-state reactions: the universality of master plots for analyzing isothermal and nonisothermal experiments. JPCA 104, 10777–10782. https://doi.org/10.1021/JP0022205.

Hameed, B.H., Tan, I.A.W., Ahmad, A.L., 2008. Adsorption isotherm, kinetic modeling and mechanism of 2,4,6-trichlorophenol on coconut husk-based activated carbon. Chem. Eng. J. 144, 235–244.

Hegde, V., Uthappa, U.T., Mane, P.V., Ji, S.M., Suneetha, M., Wang, B., Altalhi, T., Subrahmanya, T.M., Kurkuri, M.D., 2024. Design of low-cost natural casein biopolymer based adsorbent for efficient adsorption of multiple anionic dyes and diclofenac sodium from aqueous solutions. Chemosphere 353, 141571. https://doi.org/10.1016/J.CHEMOSPHERE.2024.141571.

Hernández-Zamora, M., Martínez-Jerónimo, F., 2019. Congo red dye diversely affects organisms of different trophic levels: a comparative study with microalgae, cladocerans, and zebrafish embryos. Environ. Sci. Pollut. Res. Int. 26, 11743–11755. https://doi.org/10.1007/S11356-019-04589-1.

Hokkanen, S., Bhatnagar, A., Repo, E., Lou, S., Sillanpää, M., 2016. Calcium hydroxyapatite microfibrillated cellulose composite as a potential adsorbent for the removal of Cr(VI) from aqueous solution. Chem. Eng. J. 283, 445–452. https://doi.org/10.1016/J.CEJ.2015.07.035.

Hou, H., Zhou, R., Wu, P., Wu, L., 2012. Removal of Congo red dye from aqueous solution with hydroxyapatite/chitosan composite. Chem. Eng. J. 211–212, 336–342. https://doi.org/10.1016/J.CEJ.2012.09.100.

Huang, B.C., He, C.S., Fan, N.S., Jin, R.C., Yu, H.Q., 2020. Envisaging wastewater-to-energy practices for sustainable urban water pollution control: current achievements and future prospects. Renew. Sustain. Energy Rev. 134, 110134 https://doi.org/10.1016/J.RSER.2020.110134.

Huang, H., Young, T.A., Schwab, K.J., Jacangelo, J.G., 2012. Mechanisms of virus removal from secondary wastewater effluent by low pressure membrane filtration. J. Membr. Sci. 409–410, 1–8. https://doi.org/10.1016/J.MEMSCI.2011.12.050.

Ilyas, R.A., Aisyah, H.A., Nordin, A.H., Ngadi, N., Zuhri, M.Y.M., Asyraf, M.R.M., Sapuan, S.M., Zainudin, E.S., Sharma, S., Abral, H., Asrofi, M., Syafri, E., Sari, N.H., Rafidah, M., Zakaria, S.Z.S., Razman, M.R., Majid, N.A., Ramli, Z., Azmi, A., Bangar, S.P., Ibrahim, R., 2022. Natural-fiber-reinforced chitosan, chitosan blends and their nanocomposites for various advanced applications. Polymers 14. https://doi.org/10.3390/POLYM14050874.

Jamshidifard, S., Koushkbaghi, S., Hosseini, S., Rezaei, S., Karamipour, A., Jafari rad, A., Irani, M., 2019a. Incorporation of UiO-66-NH2 MOF into the PAN/chitosan nanofibers for adsorption and membrane filtration of Pb(II), Cd(II) and Cr(VI) ions from aqueous solutions. J. Hazard Mater. 368, 10–20. https://doi.org/10.1016/J.JHAZMAT.2019.01.024.

Jamshidifard, S., Koushkbaghi, S., Hosseini, S., Rezaei, S., Karamipour, A., Jafari rad, A., Irani, M., 2019b. Incorporation of UiO-66-NH2 MOF into the PAN/chitosan nanofibers for adsorption and membrane filtration of Pb(II), Cd(II) and Cr(VI) ions from aqueous solutions. J. Hazard Mater. 368, 10–20. https://doi.org/10.1016/J.JHAZMAT.2019.01.024.

Jiang, X., 2003. Multi-scalar filtration methodologies. Advanced techniques for assessment surface topography: development of a basis for 3D surface texture standards. Surfstand 91–115. https://doi.org/10.1016/B978-190399611-9/50005-0.

Kadier, A., Al-Qodah, Z., Akkaya, G.K., Song, D., Peralta-Hernández, J.M., Wang, J.Y., Phalakornkule, C., Bajpai, M., Niza, N.M., Gilhotra, V., Bote, M.E., Ma, Q., Obi, C.C., Igwegbe, C.A., 2022. A state-of-the-art review on electrocoagulation (EC): an efficient, emerging, and green technology for oil elimination from oil and gas industrial wastewater streams. Case Studies in Chemical and Environmental Engineering 6. https://doi.org/10.1016/j.cscee.2022.100274.

Khadim, H.J., Ammar, S.H., Ebrahim, S.E., 2019. Biomineralization based remediation of cadmium and nickel contaminated wastewater by ureolytic bacteria isolated from barn horses soil. Environ. Technol. Innov. 14, 100315 https://doi.org/10.1016/J.ETI.2019.100315.

Kumar, M., Borah, P., Devi, P., 2020. Priority and emerging pollutants in water. Inorganic Pollutants in Water 33–49. https://doi.org/10.1016/B978-0-12-818965-8.00003-2.

Lateef, S.K., Soh, B.Z., Kimura, K., 2013. Direct membrane filtration of municipal wastewater with chemically enhanced backwash for recovery of organic matter. Bioresour. Technol. 150, 149–155. https://doi.org/10.1016/J.BIORTECH.2013.09.111.

Li, Y., Qi, X., Li, G., Wang, H., 2021. Double-pathway arsenic removal and immobilization from high arsenic-bearing wastewater by using nature pyrite as in situ Fe and S donator. Chem. Eng. J. 410, 128303 https://doi.org/10.1016/J.CEJ.2020.128303.

Lin, H., Li, Y., Zhu, J., 2020. Cross-linked GO membranes assembled with GO nanosheets of differently sized lateral dimensions for organic dye and chromium separation. J. Membr. Sci. 598 https://doi.org/10.1016/j.memsci.2019.117789.

Lin, Z., Jiang, W., Chen, Z., Zhong, L., Liu, C., 2021. Shape-memory and anisotropic carbon aerogel from biomass and graphene oxide. Molecules 26. https://doi.org/10.3390/molecules26185715.

Lyczko, N., Nzihou, A., Sharrok, P., 2014a. Calcium phosphate sorbent for environmental application. Procedia Eng. 83, 423–431. https://doi.org/10.1016/J.PROENG.2014.09.051.

Lyczko, N., Nzihou, A., Sharrok, P., 2014b. Calcium phosphate sorbent for environmental application. Procedia Eng. 83, 423–431. https://doi.org/10.1016/J.PROENG.2014.09.051.

Lyczko, N., Sebei, H., Nzihou, A., Sharrock, P., 2017. Treatment of municipal wastewater with calcium phosphate: a new physicochemical purification step. Environ Eng Manag J 16, 2573–2580. https://doi.org/10.30638/EEMJ.2017.267.

Ma, H., Bowman, C.N., Davis, R.H., 2000. Membrane fouling reduction by backpulsing and surface modification. J. Membr. Sci. 173, 191–200. https://doi.org/10.1016/S0376-7388(00)00360-4.

Madeira, C.L., de Araújo, J.C., 2021. Inhibition of anammox activity by municipal and industrial wastewater pollutants: a review. Sci. Total Environ. 799 https://doi.org/10.1016/J.SCITOTENV.2021.149449.

Malik, M.H., Shahzadi, L., Batool, R., Safi, S.Z., Khan, A.S., Khan, A.F., Chaudhry, A.A., Rehman, I.U., Yar, M., 2020. Thyroxine-loaded chitosan/carboxymethyl cellulose/hydroxyapatite hydrogels enhance angiogenesis in in-ovo experiments. Int. J. Biol. Macromol. 145, 1162–1170. https://doi.org/10.1016/J.IJBIOMAC.2019.10.043.

Meena, R.A.A., Yukesh Kannah, R., Sindhu, J., Ragavi, J., Kumar, G., Gunasekaran, M., Rajesh Banu, J., 2019. Trends and resource recovery in biological wastewater treatment system. Bioresour. Technol. Rep. 7, 100235 https://doi.org/10.1016/J.BITEB.2019.100235.

Mubarak, N.M., Sahu, J.N., Abdullah, E.C., Jayakumar, N.S., 2014. Removal of heavy metals from wastewater using carbon nanotubes removal of heavy metals from wastewater 2119. https://doi.org/10.1080/15422119.2013.821996.

Nayak, A., Bhushan, B., 2021. Hydroxyapatite as an advanced adsorbent for removal of heavy metal ions from water: focus on its applications and limitations. Mater. Today Proc. 46, 11029–11034. https://doi.org/10.1016/J.MATPR.2021.02.149.

Nechyporchuk, O., Yang Nilsson, T., Ulmefors, H., Köhnke, T., 2020. Wet spinning of chitosan fibers: effect of sodium dodecyl sulfate adsorption and enhanced dope temperature. ACS Appl. Polym. Mater. 2, 3867–3875. https://doi.org/10.1021/ACSAPM.0C00562/ASSET/IMAGES/LARGE/AP0C00562_0007.JPEG.

Park, S.J., Hwang, Y.-C., Oh, W., Hwang, I.-N., 2007. Opacity and masking effect of the opaque shade composite resins. Journal of Korean Academy of Conservative Dentistry 32, 356. https://doi.org/10.5395/JKACD.2007.32.4.356.

Pasquini, D., Alves Henrique, M., Gopakumar, D.A., Carlos de Morais, L., Grohens, Y., Thomas, S., n.d Meldrum's Acid Modified Cellulose Nanofiber-Based Polyvinylidene Fluoride Microfiltration Membrane for Dye Water Treatment and Nanoparticle Removal. https://doi.org/10.1021/acssuschemeng.6b02952.

Peter, S., Lyczko, N., Gopakumar, D., Maria, H.J., Nzihou, A., Thomas, S., 2022. Nanocellulose and its derivative materials for energy and environmental applications. J. Mater. Sci. 57 (13), 6835–6880. https://doi.org/10.1007/S10853-022-07070-6, 2022 57.

Peter, S., Lyczko, N., Gopakumar, D., Maria, H.J., Nzihou, A., Thomas, S., 2020. Chitin and chitosan based composites for energy and environmental applications: a review. Waste and Biomass Valorization 12 (9), 4777–4804. https://doi.org/10.1007/S12649-020-01244-6, 2020 12.

Pouya, Z.A., Tofighy, M.A., Mohammadi, T., 2021. Synthesis and characterization of polytetrafluoroethylene/oleic acid-functionalized carbon nanotubes composite membrane for desalination by vacuum membrane distillation. Desalination 503. https://doi.org/10.1016/j.desal.2021.114931.

Qasem, N.A.A., Mohammed, R.H., Lawal, D.U., 2021. Removal of heavy metal ions from wastewater: a comprehensive and critical review. npj Clean Water 4 (1), 1–15. https://doi.org/10.1038/s41545-021-00127-0, 2021 4.

Ramasamy, R., Aragaw, T.A., Balasaraswathi Subramanian, R., 2022. Wastewater treatment plant effluent and microfiber pollution: focus on industry-specific wastewater. Environ. Sci. Pollut. Control Ser. 29 (34), 51211–51233. https://doi.org/10.1007/S11356-022-20930-7, 2022 29.

Shim, B.S., Tang, Z., Morabito, M.P., Agarwal, A., Hong, H., Kotov, N.A., 2007. Integration of conductivity, transparency, and mechanical strength into highly homogeneous layer-by-layer composites of single-walled carbon nanotubes for optoelectronics. Chem. Mater. 19, 5467–5474. https://doi.org/10.1021/CM070442A/SUPPL_FILE/CM070442A-FILE002.PDF.

Soomro, F., Memon, F.H., Khan, M.A., Iqbal, M., Ibrar, A., Memon, A.A., Lim, J.H., Choi, K.H., Thebo, K.H., 2023. Ultrathin graphene oxide-based nanocomposite membranes for water purification. Membranes 13. https://doi.org/10.3390/membranes13010064.

Szatkowski, T., Kołodziejczak-Radzimska, A., Zdarta, J., Szwarc-Rzepka, K., Paukszta, D., Wysokowski, M., Ehrlich, H., Jesionowski, T., 2015. Synthesis and characterization of hydroxyapatite/chitosan composites. undefined 51, 575–585. https://doi.org/10.5277/PPMP150217.

Tang, X., Zheng, H., Teng, H., Sun, Y., Guo, J., Xie, W., Yang, Q., Chen, W., 2016. Chemical coagulation process for the removal of heavy metals from water: a review. Desalination Water Treat. 57, 1733–1748. https://doi.org/10.1080/19443994.2014.977959.

Thirunavukkarasu, A., Nithya, R., Sivashankar, R., 2020. A review on the role of nanomaterials in the removal of organic pollutants from wastewater. Rev. Environ. Sci. Biotechnol. 19, 751–778. https://doi.org/10.1007/S11157-020-09548-8/FIGURES/5.

Thomas, S., Soloman, P.A., Rejini, V.O., 2016. Preparation of chitosan- CMC blends and studies on thermal properties. Procedia Technology 24. https://doi.org/10.1016/j.protcy.2016.05.201.

Ueno, A., Suzuki, H., Kotera, Y., 1983. Particle-size distribution of nickel dispersed on silica and its effects on hydrogenation of propionaldehyde. Journal of the Chemical Society, Faraday Transactions 1. Physical Chemistry in Condensed Phases 79, 127–136. https://doi.org/10.1039/F19837900127.

Uthappa, U.T., Sriram, G., Arvind, O.R., Kumar, S., Ho-Young-Jung, Neelgund, G.M., Losic, D., Kurkuri, M.D., 2020. Engineering MIL-100(Fe) on 3D porous natural diatoms as a versatile high performing platform for controlled isoniazid drug release, Fenton's catalysis for malachite green dye degradation and environmental adsorbents for Pb2+ removal and dyes. Appl. Surf. Sci. 528, 146974 https://doi.org/10.1016/J.APSUSC.2020.146974.

van Rijt, M.M.J., Nooteboom, S.W., van der Weijden, A., Noorduin, W.L., de With, G., 2021. Stability-limited ion-exchange of calcium with zinc in biomimetic hydroxyapatite. Mater. Des. 207, 109846 https://doi.org/10.1016/J.MATDES.2021.109846.

Vatanpour, V., Jouyandeh, M., Akhi, H., Mousavi Khadem, S.S., Ganjali, M.R., Moradi, H., Mirsadeghi, S., Badiei, A., Esmaeili, A., Rabiee, N., Habibzadeh, S., Koyuncu, I., Nouranian, S., Formela, K., Saeb, M.R., 2022. Hyperbranched polyethylenimine functionalized silica/polysulfone nanocomposite membranes for water purification. Chemosphere 290. https://doi.org/10.1016/j.chemosphere.2021.133363.

Wang, Y., Chen, X., Zhang, J., Yin, J., Wang, H., 2009. Investigation of microfiltration for treatment of emulsified oily wastewater from the processing of petroleum products. Desalination 249, 1223–1227. https://doi.org/10.1016/J.DESAL.2009.06.033.

Wanyonyi, W.C., Onyari, J.M., Shiundu, P.M., 2014. Adsorption of Congo red dye from aqueous solutions using roots of Eichhornia crassipes: kinetic and equilibrium studies. Energy Proc. 50, 862–869. https://doi.org/10.1016/J.EGYPRO.2014.06.105.

Water and wastewater treatment technologies [WWW Document], n.d. URL https://www.nature.com/collections/bggcjhebai (accessed 1.April.2023).

Weißpflog, J., Vehlow, D., Müller, M., Kohn, B., Scheler, U., Boye, S., Schwarz, S., 2021. Characterization of chitosan with different degree of deacetylation and equal viscosity in dissolved and solid state – insights by various complimentary methods. Int. J. Biol. Macromol. 171, 242–261. https://doi.org/10.1016/J.IJBIOMAC.2021.01.010.

Weng, R., Chen, L., Lin, S., Zhang, H., Wu, H., Liu, K., Cao, S., Huang, L., 2017. Preparation and characterization of antibacterial cellulose/chitosan nanofiltration membranes. Polymers 9, 116. https://doi.org/10.3390/POLYM9040116, 2017, Vol. 9, Page 116.

Yang, Z., Li, L., Jiang, C., Zhao, N., Zhang, S., Guo, Y., Chen, Y., Xue, S., Ji, C., Zhao, S., Gonzales, R.R., Matsuyama, H., Xia, J., Niu, Q.J., 2021. Tailored thin film nanocomposite membrane incorporated with Noria for simultaneously overcoming the permeability-selectivity trade-off and the membrane fouling in nanofiltration process. J. Membr. Sci. 640 https://doi.org/10.1016/j.memsci.2021.119863.

Yanti, P.H., Pebrianti, R., 2021. Microwave-assisted of synthesis and characterization of nanocomposite hydroxyapatite-chitosan. J Phys Conf Ser 1842, 012048. https://doi.org/10.1088/1742-6596/1842/1/012048.

Yurekli, Y., 2016. Removal of heavy metals in wastewater by using zeolite nano-particles impregnated polysulfone membranes. J. Hazard Mater. 309, 53–64. https://doi.org/10.1016/J.JHAZMAT.2016.01.064.

Zeng, G., He, Y., Zhan, Y., Zhang, L., Pan, Y., Zhang, C., Yu, Z., 2016. Novel polyvinylidene fluoride nanofiltration membrane blended with functionalized halloysite nanotubes for dye and heavy metal ions removal. J. Hazard Mater. 317, 60–72. https://doi.org/10.1016/J.JHAZMAT.2016.05.049.

Zhang, X., Wang, X., 2015. Adsorption and desorption of nickel(II) ions from aqueous solution by a lignocellulose/montmorillonite nanocomposite. PLoS One 10, e0117077. https://doi.org/10.1371/JOURNAL.PONE.0117077.

Zhang, Q.H., Yang, W.N., Ngo, H.H., Guo, W.S., Jin, P.K., Dzakpasu, Mawuli, Yang, S.J., Wang, Q., Wang, X.C., Ao, D., 2016. Current status of urban wastewater treatment plants in China. Environment International 92-93, 11–22. ISSN 0160-4120. https://doi.org/10.1016/j.envint.2016.03.024.

Zhang, Y., Wu, B., Xu, H., Liu, H., Wang, M., He, Y., Pan, B., 2016. Nanomaterials-enabled water and wastewater treatment. NanoImpact. https://doi.org/10.1016/j.impact.2016.09.004.

Zhao, G., Lyu, X., Lee, J., Cui, X., Chen, W.N., 2019. Biodegradable and transparent cellulose film prepared eco-friendly from durian rind for packaging application. Food Packag. Shelf Life 21, 100345. https://doi.org/10.1016/J.FPSL.2019.100345.

Zhu, H.Y., Jiang, R., Xiao, L., 2010. Adsorption of an anionic azo dye by chitosan/kaolin/γ-Fe2O3 composites. Appl. Clay Sci. https://doi.org/10.1016/j.clay.2010.02.003.

Zhu, J., Tian, M., Zhang, Y., Zhang, H., Liu, J., 2015. Fabrication of a novel "loose" nanofiltration membrane by facile blending with Chitosan–Montmorillonite

nanosheets for dyes purification. Chem. Eng. J. 265, 184–193. https://doi.org/10.1016/J.CEJ.2014.12.054.